Journal of the European Ceramic Society 23 (2003) 469–479

www.elsevier.com/locate/jeurceramsoc

Fractal analysis of cracks in alumina–zirconia composites

Annamaria Celli*, Antonella Tucci, Leonardo Esposito, Carlo Palmonari

Italian Ceramic Center, Via Martelli 26, 40138 Bologna, Italy

Received 25 May 2001; accepted 5 May 2002

Abstract

The crack paths, induced by Vickers indentation in alumina–zirconia composites, were analyzed using fractal geometry. The fractal dimension n_S was calculated for each crack. This parameter refers to a corresponding three-dimensional fracture surface and indicates how its geometry varies by changing the magnification. An interesting correlation between K_{IC} and n_S was found: it suggests that the samples with high percentages of alumina and also the pure zirconia are characterized by an intergranular fracture mode, while the composites with high zirconia content present a transgranular fracture mode. This result is confirmed by analyzing the energies of fracture calculated using both the classical and fractal approaches. The results obtained in this research not only made it possible to understand the fracture behavior of the analyzed composites, but also confirmed the good potential of fractal analysis to explain complex mechanisms such as those involved in the fracture of brittle materials.

Keywords: Al_2O_3; Al_2O_3–ZrO_2; Composites; Crack path; Fractal analysis; Toughening; Toughness; ZrO_2

1. Introduction

Fracture processes can be very difficult to understand, but understanding these processes plays a significant role in avoiding mechanical failure in materials applications, especially with brittle materials such as ceramics. In materials science a method of investigating fracture mechanisms is the analysis of the result of fracture. The geometrical characteristics of fracture surfaces (depth, roughness, curvature, etc.) are analyzed using projected two-dimensional images obtained by light and electron microscopy[1–5] or, more recently, using three-dimensional images obtained by atomic force microscopy.[6] At the microscopic level the crack paths are also studied and their nonlinearity is often found. Deflection or branching phenomena can occur, caused by several factors such as local stress state, microstructure discontinuities (second phases, grain boundaries, inclusions, etc.) or environment.[7–11] Determination of the effective crack geometry is sometimes essential to better understand the toughening mechanisms of brittle solids[10] or fatigue resistance[7] or the role of microstructure in fracture processes.[11]

In the light of such experimental evidence, over the last few years much work has been directed towards obtaining quantitative descriptions of the geometric characteristics of cracks: tortuosity parameters[1,7,9] or universal exponents, referring to the scale invariance of crack roughness,[12,13] have been proposed. Recently, a new tool, based on fractal concepts, has also been developed to analyze and quantify the fracture modes[14,15] and geometric characteristics of cracks.[16–19]

Fractal geometry, introduced by Mandelbrot in 1977,[20,21] is a non-Euclidean geometry, allowing the study of irregular shapes and chaotic phenomena present in nature. It is able to describe, in a very concise manner, objects characterized by the properties of self-affinity or self-similarity. Fracture is a phenomenon that has been modeled using fractal geometry: the topography and the geometric characteristics of the fracture surfaces of metals,[22] ceramics [23,24] and polymers[25] have been quantitatively described. In particular, the fracture of brittle materials has been found to be a self-similar and scale invariant process, where self-similarity means that multiple features of objects appear always the same and scale invariance means that a feature at one level of magnification is related to another feature at

* Corresponding author: Dipartimento di Chimica Applicata e Scienza dei Materiali, Facoltà di Ingegneria, Viale Risorgimento 2, Bologna, Italy. Fax: +39-051-209-3218.

E-mail address: annamaria.celli@mail.ing.unibo.it (A. Celli).

0955-2219/02/$ - see front matter
PII: S0955-2219(02)00148-6

another magnification through a scalar magnification constant.[14,26]

This analytical approach, widely discussed[26–29] after the first works of Mandelbrot, represents a new way to quantitatively express (by an exponent, the fractal dimension D) the characteristics of an irregular surface: D is not simply a roughness parameter, but refers to the way in which all the geometrical features of the fractal object change when the observation scale changes. By analyzing the fracture surfaces for several ceramic materials, a direct correlation between the fracture toughness K_{IC} and the fractional part of the fractal parameter, D^*, has been found:[14,23,24]

$$K_{IC} = K_0 + AD^{*0.5} \tag{1}$$

where A is a constant for families of materials having similar microstructural features and contains a term that describes the fracture process at the atomic level. Therefore, by observing the fracture effects at a microscopical scale (micron level), it is possible to extrapolate the phenomena to the atomic level (angstrom level). In this way interesting indications about the fracture mechanisms can be obtained and the understanding of fracture processes can be remarkably improved.

Even though, generally, fractal analysis is used to quantitatively characterize three-dimensional objects (fracture surfaces), in the present study it is applied to the two-dimensional case, fracture cracks. The profiles of cracks, obtained on the surfaces of ceramic materials, an alumina, a zirconia (Y-TZP) and mixtures of the two oxides, covering a wide compositional range, were analyzed.

For this class of materials, the fracture mechanisms and the relationships between mechanical properties and microstructure are very complex, because several fracture mechanisms can be involved, such as martensitic transformation of zirconia from the tetragonal to monoclinic phase,[30] crack deflection,[31] microcrack formation,[32–34] and crack bridging.[35] For these materials the influence of their microstructure on the mechanical behavior is very important. For example, the size of the grains strictly influences the efficiency of the martensitic transformation mechanism.[35–37] and/or the development of microcracks.[32] Several papers have been published on these topics,[30–39] and there is some discrepancy about the effect of the addition of zirconia in alumina and alumina in zirconia on the mechanical properties. Such discrepancies can be attributed to the difference in the starting materials and/or processing, which influence the final microstructure and the crystalline phases.

In view of these problems, the aim of this work was to explore a new method of study, quantitative analysis of the crack geometry based on fractals, in order to check if this approach can be useful to better understand the fracture mechanisms of this class of materials.

2. Fractal dimension determination

The fractal geometry is able to describe an irregular object by its dimension, that is a fractional number varying between the corresponding euclidean dimension and the dimension of the space in which the object is embedded. For example, an irregular curve is characterized by a fractal dimension varying between 1 and 2 and an irregular surface by a fractal dimension varying between 2 and 3.

The problem of determining the fractal dimension was firstly discussed by Mandelbrot,[20,21] who observed that the measure of the length of an irregular curve is a function of the scale used to measure it. When the magnification is increased or the size of the measuring unit decreased, the length increases without limit. Then, the dependence of the measured length (L) from the measuring unit (η) is expressed by Eq. (2):

$$L(\eta) = L_0\eta^{-(D-1)} \tag{2}$$

where L_0 is a constant with the dimension of L and D represents the fractal dimension of the curve. $(D-1) = D^*$ is the fractional part of the fractal parameter of the irregular profile. The linear form of Eq. (2), described by the Eq. (3):

$$\ln L(\eta) = \ln L_0 - D^* \ln \eta \tag{3}$$

allows one to easily obtain the D^* value, from the slope of the straight line obtained in the plot of ln $L(\eta)$ vs. ln η, known as the Richardson plot.

However, Underwood et al.[40,41] pointed out as the linearity expected in the Richardson plot is not often obtained: L, that could increase without limit for $\eta \to 0$, often tends to a limit value for small values of η. Therefore, the plot of ln $L(\eta)$ vs. ln η assumes a sigmoidal trend. Underwood et al., in order to linearize this plot, introduced the roughness term R_L corresponding to the ratio between the real length L and the projected length L_0: R_L presents the same dependence as that of L from η, expressed by Eq. (4), showing a sigmoidal trend:

$$R_L = R_{L0}\eta^{-D^*} \tag{4}$$

The linearization of Eq. (4) was obtained by Underwood and co-workers[40,41] by the following expression:

$$\log \log\left[\frac{(R_L)_0 - (R_L)_\infty}{R_L(\eta) - (R_L)_\infty}\right] = \log\left(\frac{\alpha}{2.3}\right) \pm \beta \log \eta \tag{5}$$

where $(R_L)_0$ and (R_L) represent the asymptotes of R_L as $\eta \to 0$ and $\eta \to \infty$ respectively, α and β are constants and $D_\beta = \beta + 1$ is a new fractal parameter. This latter is seen as more effective than the conventional parameter D in describing the geometry of an irregular curve.[40,41]

However, the application of Eq. (5) to linearize our experimental data, log R_L vs. log η, for the Al_2O_3–ZrO_2 composites and for another class of materials, Si_3N_4–SiC_w composites,[42,43] didn't give the expected linear trend: therefore a different approach was proposed by the authors.[42,43] For an irregular profile, the equation proposed is:

$$\log\left[-\log\frac{\log\ R_L(\eta)}{\log\ (R_L)_0}\right] = \log\ K' + n\log(\log\eta) \tag{6}$$

where n, lower than 1, represents the fractional part of the fractal parameter for a curve. It is also possible to determine the fractal parameter of the fracture surface characterized by the same geometrical characteristics of the crack path: this procedure assumes that the geometry of the crack profile can be extrapolated to three-dimensionality. For a fractal surface the proposed equation is:[42,43]

$$\log\left[-\log\frac{\log\ R_S(\eta^2)}{\log(R_S)_0}\right] = \log K'' + \mathrm{ns}\ \log\ \log(\eta^2) \tag{7}$$

where R_S is the ratio between the real surface area $S(\eta^2)$ and its projected area. R_S represents the surface roughness and is calculated by the Eq. (8):[40,41]

$$R_S = \frac{4}{\pi}(R_L - 1) + 1 \tag{8}$$

Log $(R_S)_0$ is the asymptotic value of log $R_S(\eta^2)$ when log $(\eta^2)\to 0$ and n_S, which varies between 0 and 1, represents the fractional part of the surface fractal parameter.

Therefore, from the roughness data (R_L) of a crack, by combination of Eqs. (8) and (7), it is possible to obtain the fractal surface parameter n_S. This method, already validated because it was able to recognize different fracture mechanisms in ceramic-whiskers composites,[42,43] has the advantage of being relatively very simple from an experimental point of view: it does not require complex analyses of the three-dimensional geometry of fracture surfaces, but only two-dimensional images of cracks.

3. Experimental procedure

The materials tested were sintered single oxides, alumina, A, and 3% mol. yttria-stabilized zirconia, Z, as well as mixed oxides, homogeneous mixtures of 3% mol. yttria-stabilized zirconia and different percentages of alumina, 20, 40, 60 and 80 wt.%, denominated 20A, 40A, 60A, and 80A, respectively. The samples were formed using a colloidal shaping technique[44] starting from commercial powders, A (SM8 Baikowski, France), Z (TZ 3YS, Tosoh, Japan) and the mixed oxides (all supplied by Tosoh, Japan). The sintering of the green compacts, carried out in air and in the temperature range 1500–1600 °C depending on their composition, allowed a nearly theoretical density to be reached. Observations of the sintered materials by scanning electron microscopy (SEM) showed highly homogeneous microstructures without agglomerates, pores or abnormally grown alumina grains. X-ray diffraction analysis of the samples indicated that only α-alumina and tetragonal zirconia are the crystalline phases present in both the pure samples and in the composites.

For all the tested materials, the average size of the alumina and zirconia grains was determined from SEM images of randomly selected areas of the polished and thermally etched specimens using suitable software (Leica Qwin Imaging System). Because the tested materials were characterized by rounded, equiaxed grains, the diameter of the circle, having the same area as that of the grain, was used as the characteristic grain size parameter.[45] The average value was obtained based on the analysis of at least 150 grains for each material.

After an accurate surface polishing operation, that completely eliminated the surface residual stresses, as detected by X-ray diffraction analysis, the fracture mechanisms were studied by analyzing the cracks emerging from the corners of Vickers impressions, using a hardness tester (Zwick 3212, Germany) and applying a load of 98.1 N for 18 s. Fracture toughness, K_{IC}, was determined using the direct crack measurement method with the Anstis equation.[46] The cracks, emerging from the indentation corners, were observed by SEM and the corresponding micrographs, all taken at the same magnification, were digitalised and the crack profiles were elaborated by image analysis in order to determine the fractal parameter.

Young's modulus was determined using a four point bending apparatus equipped with an extensometer (MTS M 10 machine, USA).

4. Results and discussion

4.1. Analysis of the microstructure

All the sintered materials, pure oxides and composites, are characterized by very high density, ranging from 99.5 to 100% TD, Table 1. In the mixed oxides a high degree of homogeneous dispersion, in terms of Al_2O_3 and ZrO_2 grains, is observed. Concerning the grain size, some differences are evident, as a function of their composition. Table 2 reports the average size of alumina and zirconia grains for the tested samples. The alumina grains in the pure alumina A, having the average value of 3.4 μm, are the largest of all the materials examined. In 80A the alumina grains are larger than the zirconia grains. While 40A and 60A show a similar

Table 1
Material characteristics

Material	Z	20A	40A	60A	80A	A
Density (g cm^{-3})	6.05	5.48	5.02	4.60	4.27	3.95
K_{IC} (MPa $m^{0.5}$)	4.3±0.1	5.0±0.2	5.2±0.1	3.6±0.2	4.1±0.4	4.2±0.4
E(GPa)	201	246	285	316	348	356

Table 2
Average grain size of the materials examined

Material	Z	20A	40A	60A	80A	A
Al_2O_3 (μm)	–	0.68	0.29	0.37	0.60	3.4
ZrO_2 (μm)	0.74	0.60	0.36	0.25	0.25	–

microstructure, characterized by the presence of alumina and zirconia grains with very near submicronic average grain sizes, 20A has larger grains of both alumina and zirconia. These differences in microstructure must be taken into account to understand the fracture mechanisms.

4.2. Mechanical properties

Table 1 reports the fracture toughness, K_{IC}, and Young's modulus, E, values for the tested samples and Fig. 1 shows the trend of fracture toughness as a function of the alumina content. Starting from the pure zirconia, K_{IC} increases with increasing alumina content, reaching the maximum value for 40A, and then decreases considerably. It is noteworthy that the pure oxides, Z and A, show similar values of K_{IC}, 4.2–4.3 MPa $m^{1/2}$, and that the composites 40A and 60A, characterized by very similar sizes of the alumina and zirconia grains, are characterized by the largest difference in K_{IC}.

It is well known that the addition of alumina to yttria-stabilized tetragonal zirconia polycrystals, Y-TZP, justified by the advantage of obtaining a material with a higher Young's modulus and finer structure, generally produces ceramics with improved toughness. Glass and Green[31] explained the increment of K_{IC}, from pure zirconia to composites containing 4 vol.% Al_2O_3, to a toughening process of the grain boundaries of zirconia, due to the presence of aluminum impurities, and, consequently, an increment in the transgranular fracture mode. Lange,[30] on the other hand, observed that the addition of alumina to zirconia causes an increment in K_{IC}, but not so high as expected by the theory. This lack of agreement was attributed to an incomplete retention of the tetragonal phase of zirconia, to smaller grain size and/or to compositional differences. In any case, Lange emphasized that the K_{IC} of these materials was strongly influenced by the extent of the zirconia transformation.

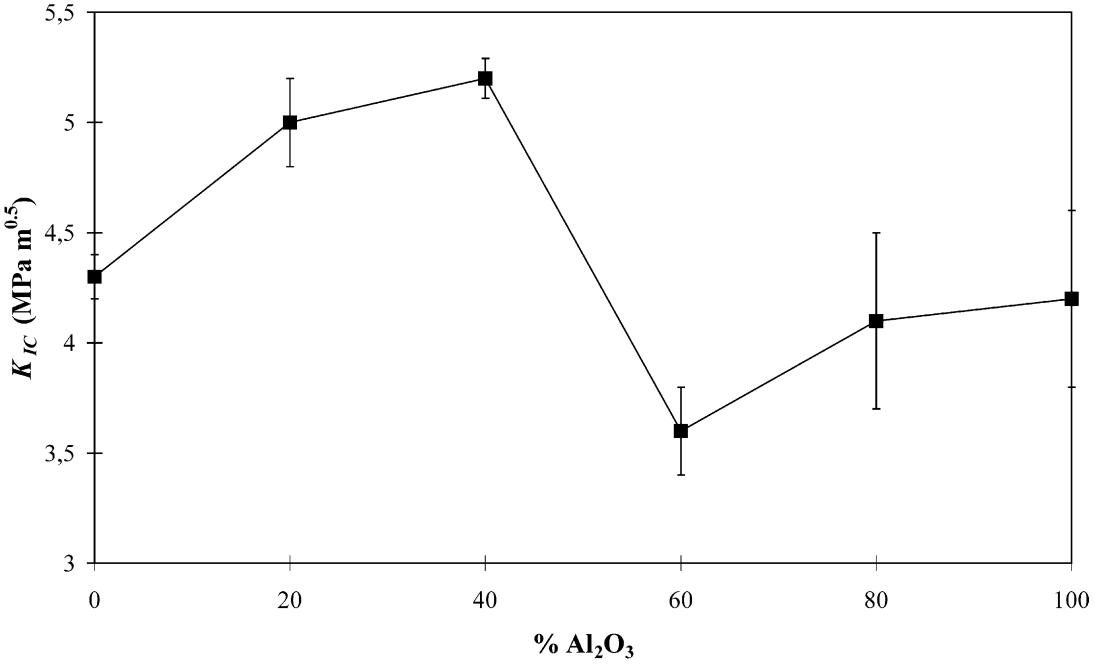

Fig. 1. Fracture toughness as a function of the alumina content for the materials examined.

Toughening mechanisms, such as crack bridging and crack deflection, may also be activated when alumina is added to Y-TZP as a dispersed second phase.

On the other hand, in the composites with a high percentage of alumina, the increase in the tetragonal zirconia content generally involves a considerable increase in K_{IC}. For Tomaszewski[39] this is due to the phase transformation of zirconia; Hori[34] hypothesizes other mechanisms, such as microcrack formation or crack ramification. Srdic,[36] comparing composites obtained by different sintering cycles, concludes that the increment in the fracture toughness is mainly related to the presence of a (i) more homogeneous structure, (ii) higher fraction of t-ZrO_2, and (iii) higher density. In any case, the trend reported in the right part of Fig. 1, where K_{IC} decreases with the addition of zirconia, is not in agreement with the results reported in the literature.

Therefore, in view of these discrepancies among experimental data and these different interpretations of the same phenomenon, an understanding of the fracture mechanisms acting in the analyzed composites requires a more in-depth analysis.

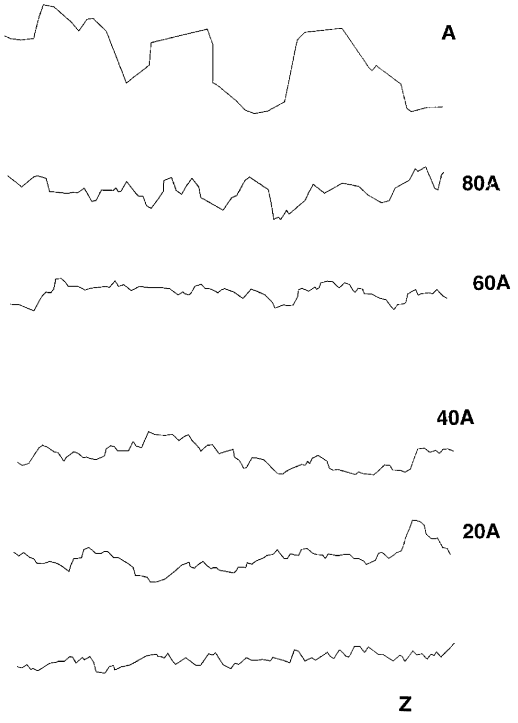

Fig. 2. Example of crack paths for the materials examined.

4.3. Analysis of the crack geometry

For each tested material the sketch of a typical segment of a crack, emerging from the indentation corner, is reported in Fig. 2. It is very clear that the crack shapes strongly depend on the material composition. However, even though from a qualitative point of view, the cracks look very different from each other, especially for the samples with a high percentage of alumina, it is necessary to carry out a quantitative analysis to evidence the true differences in their geometric characteristics.

First of all, the roughness parameter $(R_L)_0$, that represents the tortuosity of the crack, was calculated by extrapolation of log R_L to log $\eta \rightarrow 0$. R_L reflects the fractal concept of the dependence of the roughness on

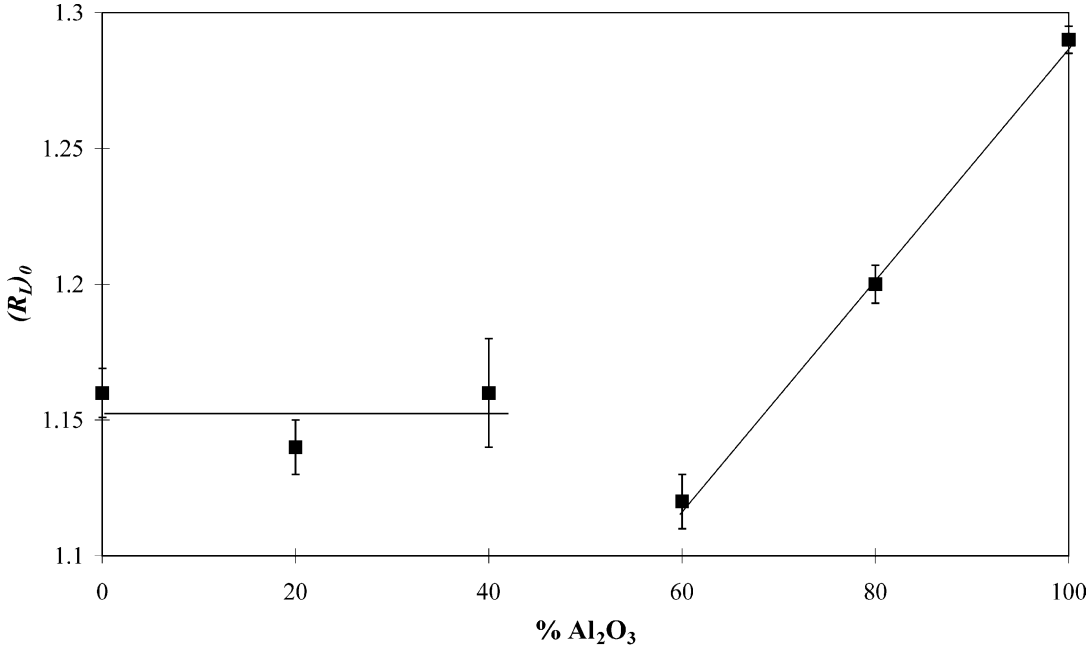

Fig. 3. Roughness parameter, $(R_L)_0$, as a function of the alumina content for the materials examined.

Table 3
Average length of the linear segments, l, and average number of crack deflections per unit length, d, present along the crack path for the materials examined

Material	Z	20A	40A	60A	80A	A
l (μm)	0.21	0.16	0.18	0.18	0.20	0.33
d (μm^{-1})	80	104	97	91	87	58

the unit length, η, used to measure it, and its extrapolation, $(R_L)_0$, allows one to avoid the dependence on the magnification. The trend of $(R_L)_0$ as a function of the percentage of alumina in the different materials is reported in Fig. 3. The samples with a high percentage of alumina show a drastic variation of $(R_L)_0$, that decreases considerably from A to 60A. For these samples, an analogous decrease in the average size of the alumina grains, the main phase for these compositions, is also observed in Table 2. Therefore, it is possible to assume that the tortuosity of the crack path decreases as the alumina grain size decreases and, then, that the cracks tend to follow the alumina grain boundaries. The same fracture mode has been observed in differently grained alumina materials.[47]

In order to have other evidence supporting this conclusion, a 'classical' quantitative analysis of the crack geometry was carried out. Table 3 reports the average length of the straight segments, l, and the average number of deviations, d, present along the crack path. It is noteworthy that, from A to 60A, l decreases and d increases in correlation with the decrease in the alumina grain dimensions. This confirms that a crack deflection mechanism takes place and gives a crack profile corresponding to the sample microstructure. The average distribution of the deviation angles was also calculated and is graphically reported in Fig. 4. From A to 60A, the percentage of small deviation angles, in the range between 10 and 20°, increases from 34% in A to 43% in 80A and to 51% in 60A. Then, the cracks for A are characterized by a small number of deviations at large angles and a very tortuous path, explaining the high efficiency of the deflection mechanism and a relatively high value of fracture toughness. In 80A and 60A the number of crack deviations decreases and the deflection angles are generally smaller. These results indicate that the crack deflection is less effective in the toughening process,[42] which in turn explains the decrease in K_{IC} in the right part of Fig. 1 and the fact that the lowest value of K_{IC} was found for 60A. Therefore, for the tested composites with a high alumina content, the introduction of zirconia does not seem to influence the toughness values.

The materials with a high zirconia content, Z, 20A and 40A, are characterized by a nearly constant value of $(R_L)_0$, as shown in Fig. 3, where it can be seen that the tortuosity of the cracks does not change in spite of the variation in the composition and microstructure. Moreover, also the lack of correlation among l, d, and deviation angle distribution on one hand and grain size on the other suggests that the intergranular fracture can not be the main fracture mechanism for these materials. Therefore, in this case, the geometry of the cracks, analyzed by traditional parameters, does not seem critical in order to suggest possible fracture mechanisms.

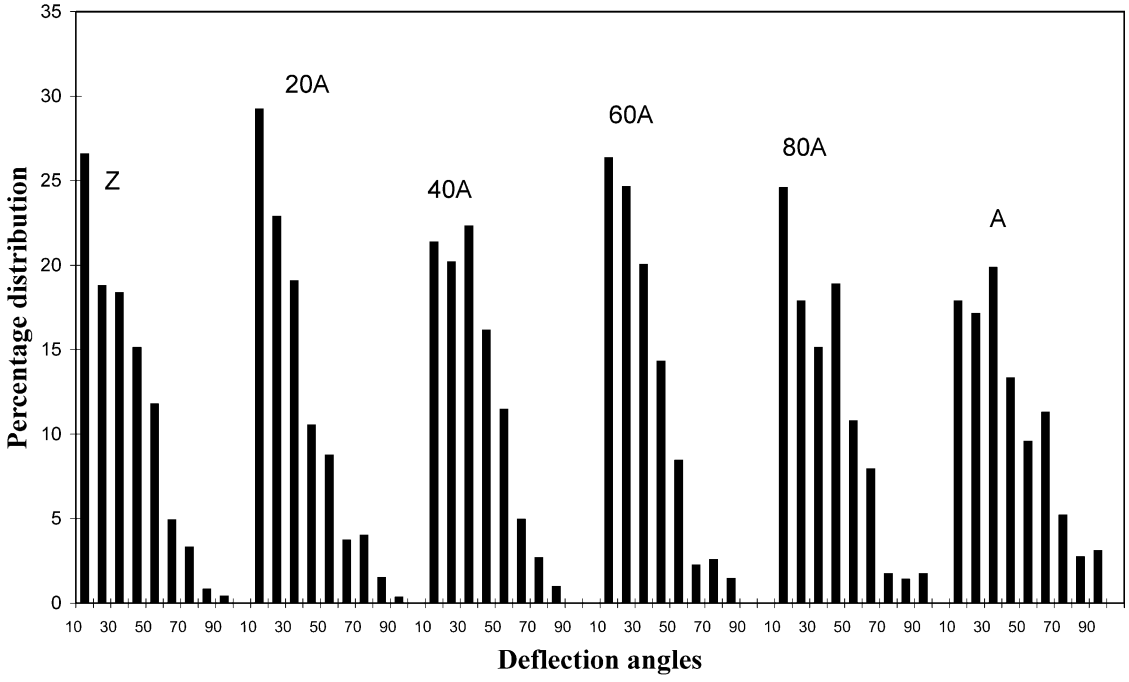

Fig. 4. Percentage of the deflection angles of the cracks developed on the surfaces of the materials examined.

4.4. Relationship between fractal parameter and fracture toughness

Fig. 5 reports K_{IC} values versus the fractal parameter $(n_S)^{0.5}$ for the analyzed materials, together with some results of the Authors on Si_3N_4–SiC_W composites[42,43] and some data from the literature.[23,24] For the latter, the fractal parameter used is D^*, that has been directly calculated by analyzing the fracture surfaces. It is possible to observe that the fractal parameter n_S is consistent with the D^* values and that the fracture toughness increases as the corresponding n_S increases for all our materials, in agreement with the geometry of fracture surfaces. In general, the more complex and irregular the crack geometry and fracture surfaces, the higher the fracture toughness.

The existence of a linear correlation between K_{IC} and the surface fractal parameters has been widely discussed in the literature[14,23,24,48–50] and seems very significant in order to define the fracture behaviors of different materials or of the same material with different microstructures. The linear correlation, found for numerous materials, such as polycrystalline ceramics, glass-ceramics and single crystals, is expressed by the equation:

$$K_{IC} = K_0 + \left[E(a_0)^{0.5}\right] D^{*0.5} \quad (9)$$

where E is the Young's modulus, K_0 is the toughness value for a smooth planar fracture and a_0 is a characteristic length involved in the fracture process. The materials are divided into classes, characterized by the same value of $[E(a_0)^{0.5}]$, corresponding to similar microstructural features and similar behaviors during fracture.

In the case of the alumina–zirconia composites, even though the data obtained in the present study alone do not clearly evidence a linear correlation between K_{IC} and n_S, when combined with other data from the literature evidence of a particular trend is found. This is a normal procedure followed when there is not a large number of data points.[50] Therefore, two different straight lines can be drawn to interpolate all the data; if the lines are extended to n_S or D^* equal to 0, they intersect approximately at the origin, confirming that the value of K_0 is nearly zero, as already found for glass ceramics[24,50] This is interpreted by the fact that there are no planar fractures for these materials, due in part to thermal vibrations occurring during the initiation of the fracture and causing a non-planar crack front.

It is noteworthy that the samples considered here belong to two different 'families', Fig. 5. A, 80A, 60A and Z belong to one 'family' of materials described in the literature, where the fracture behavior is controlled by crack deflection. This conclusion confirms our previous observations for A, 80A and 60A samples. On the other hand, 20A and 40A belong to a different 'family' of materials, together with the composites Si_3N_4–SiC_W with a high percentage of whiskers.

Since a typical fracture mechanism is characteristic for a material class, the first interesting consideration from Fig. 5 is that pure zirconia, Z, belonging to the same family of alumina based composites, should be characterized by the intergranular fracture mode. By analyzing the crack geometry only by a classical approach, it was not possible to obtain the same result,

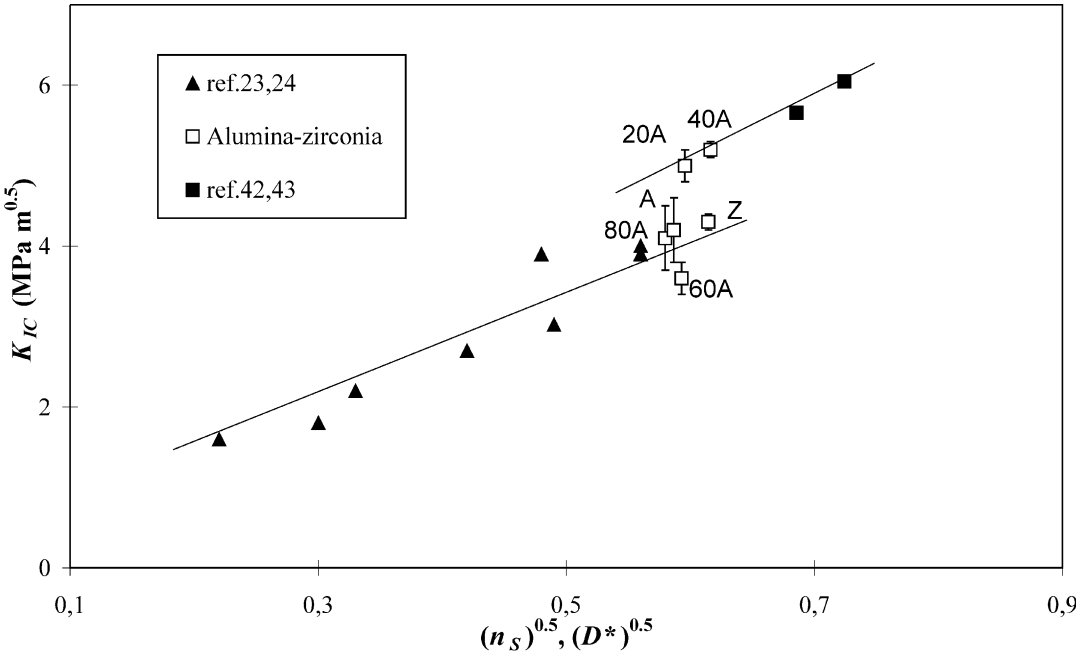

Fig. 5. Fracture toughness, K_{IC}, of the materials examined as a function of the fractal parameters n_S and D^*.

Table 4
Fracture energies γ_C and γ_F

Material	Z	20A	40A	60A	80A	A
γ_C[a] (J m^{-2})	49	13	13	30	26	23
γ_F[b] (J m^{-2})	46	49	49	21	25	23

[a] Calculated using Eq. (10).
[b] Calculated using Eq. (11).

e.g. that Z shows a fracture behavior similar to that of the materials with a high percentage of alumina and different from that of the composites with a high zirconia content.

Even though there is not a large number of experimental data points, the slopes of the two straight lines in Fig. 5 can be calculated in order to obtain the values of a_0, the atomic length related to the breaking process

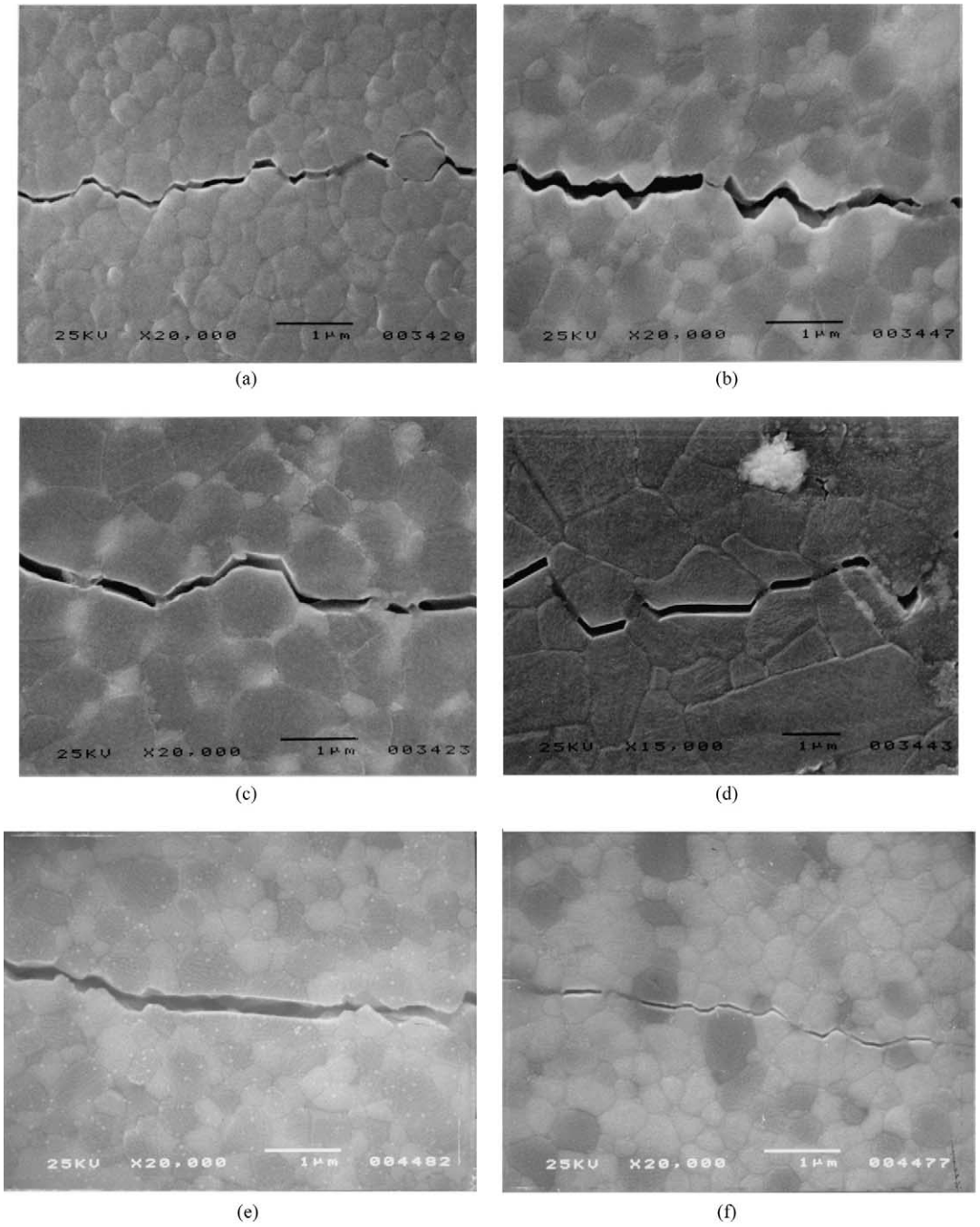

Fig. 6. SEM micrographs of the cracks induced on the surfaces of (a) Z material, (b) 60A material, (c) 80A material, (d) A material, (e) 20A material and (f) 40A material.

that controls the fracture. For 20A and 40A, a_0 varies in the range of 2.5–3.0 Å, for the other materials a_0 varies in the range 4.0–12.0 Å. These values are very similar and suggest that the same fracture mechanism acts at the atomic level for all the materials tested, corresponding to the breaking of atomic bonds.[14,51] This result is expected because the materials are characterized by the same chemical composition and crystalline structures. The differences in K_{IC} vs n_S trend for the two sample groups suggest that the materials are dissimilar only at the level of microstructure and that this is the difference that influences the behavior during fracture.

Using the a_0 values, it is possible to calculate the fracture energy γ_C, i.e. the energy/unit area required to form new crack surfaces, by Eq. (10):[51]

$$\gamma_C = \frac{a_0 D^*}{2} E \tag{10}$$

This very interesting equation correlates the macroscopic energy γ_C to the atomic energy (Ea_0) through the geometrical parameter D^* (or n_S in our case). Since fractal analysis is based on a geometrical approach, γ_C represents the contribution to the fracture energy due to only the fracture mechanisms that strongly influence the geometry of the cracks, such as crack deflection. In order to evaluate this contribution, γ_C can be compared to the corresponding total fracture energy γ_F, calculated using the classical equation [Eq. (11)]:

$$\gamma_F = (K_{IC})^2/2E \tag{11}$$

The values of γ_C and γ_F for the materials tested are reported in Table 4. The two sets of data are in good agreement, with the exception of the values obtained for 20A and 40A. The agreement between γ_C and γ_F confirms that Z, 60A, 80A and A are characterized by a fracture mechanism in which the geometrical effects are very significant. Then, crack deflection is the fracture mode that allows one to interpret all the experimental results for these samples. Also for the zirconia, the good agreement between γ_C and γ_F confirms that some other important mechanisms, such as the martensitic transformation, do not play a significant role, as already observed by the Authors for this sample using atomic force microscopy analysis.[52] Moreover, also in the literature, intergranular fracture has been reported as the main fracture mode for some samples of tetragonal zirconia.[53]

On the other hand, the composites 20A and 40A are characterized by low values of γ_C in comparison with γ_F and with γ_C obtained for the other materials. This experimental evidence confirms that these samples belong to a second family of materials, characterized by a different fracture mechanism at a microscopic level. In particular, for these samples, it is possible to assume a fracture mechanism that causes a high value of K_{IC} without inducing strong geometrical variations in the crack geometry. Transgranular fracture can occur, for example, and crack deflection probably is only a secondary process.

To confirm this hypothesis, the amount of intergranular and transgranular fractures was evaluated for each sample, by SEM observations of cracks introduced on their thermally etched surfaces. The SEM observations clearly indicate that Z, 60A, 80A and A are characterized essentially by an intergranular fracture mode (Fig. 6a–d), while 20A and 40A are mainly characterized by a transgranular fracture mode (Fig. 6e and f). Similar behavior has been observed by Glass and Green,[31] who found that the addition of a small amount of alumina (4%) in zirconia caused toughening of the zirconia grain boundaries, inducing transgranular fractures and, then, an increment in K_{IC}.

Therefore, the materials belonging to the two families, as reported in Fig. 5, show two different fracture mechanisms, intergranular and transgranular modes. From this conclusion, it is possible to explain the fracture toughness trend reported in Fig. 1: for the samples with a high percentage of alumina, right side of Fig. 1, the deflection mechanism predominates and K_{IC} decreases as a function of the alumina grain size. For 20A and 40A the transgranular fracture mode prevails and K_{IC} increases as a function of the alumina content, that induces a toughening of grain boundaries. For Z, K_{IC} is only a function of the particular microstructural characteristics of the sample and it is not comparable with the K_{IC} values found for 20A and 40A because the main fracture mechanism is not the same.

5. Conclusions

In this study fractal analysis was applied to the description of crack geometry, using a very simple experimental approach: cracks were introduced on the polished surfaces of materials and, then, their profiles analyzed by an image analysis program. A fractal parameter, n_S, that describes the geometry of the corresponding fracture surfaces, was calculated from the crack geometry. The values of n_S are in agreement with the fractal dimension values (D^*) reported in the literature and measured, by complex procedures, directly on fracture surfaces.

For the alumina–zirconia composites a relationship between fracture toughness and fractal dimension n_S was found. It was possible to identify two different families of materials and two different fracture processes. Intergranular fracture was found for pure zirconia, pure alumina and for the composites with a high percentage of alumina. In this family a significant relationship between microstructure, crack path and toughness is evident: the

larger the alumina grains, the more rough and irregular the geometry of the crack and the fracture surface, due to the crack deflection mechanism, and the higher the K_{IC}.

On the contrary, in the composites with a high zirconia content transgranular fracture was the main fracture mechanism. The energies involved in the fracture confirm this behavior. However, even though these two families of materials are characterized by different mechanical behavior at the microscopic scale, they have the same fracture mode at the atomic level, that corresponds to the breaking of the atomic bond. This is due to the fact that the crystalline structures and the chemical composition are the same for all the materials analyzed. Therefore, only differences in microstructure cause the differences in fracture mechanisms inside the composites analyzed.

In conclusion, the use of fractals to describe cracks presents the same good potential for achieving a better understanding of fracture behavior as that found for the application of fractals to fracture surfaces. The cracks represent a two-dimensional image of the corresponding fracture surface and the quantitative description of its geometrical characteristics by the fractal parameter evidences the relationship between fracture behavior and microstructure even in complex systems such as those of the composite materials examined.

References

1. Underwood, E E. and Banerji, K., Quantitative fractography. In *ASM Handbook*, *Vol. 12, Fractography*. ASM International, 1992, pp.193–210.
2. Banerji, K., Quantitative fractography: a modern perspective. *Metallurgical Transaction A*, 1988, **19A**, 961–971.
3. Chesnutt, J. C. and Spurling, R. A., Fracture topography-microstructure correlations in the SEM. *Metallurgical Transaction A*, 1977, **8A**, 216–217.
4. Fior, G. O. and Morris, J. W. Jr., Characterization of cryogenic Fe-6Ni steel fracture modes: a three dimensional quantitative analysis. *Metallurgical Transaction A*, 1986, **17A**, 815–822.
5. Healey, J T. and Mecholsky, J J. Jr., Scanning electron microscopy techniques and their application to failure analysis of brittle materials. In *Fractography of Ceramics and Metal Failures*, ASTM STP 827, ed. J J. Mecholsky Jr. and S R. Powell Jr., 1984, pp. 157–181.
6. Rädlein, E. and Frischat, G. H., Atomic force microscopy as a tool to correlate nanostructure to properties of glasses. *J. Non-Cryst. Solids*, 1997, **222**, 69–82.
7. Suresh, S., Crack deflection: implications for the growth of long and short fatigue cracks. *Metallurgical Transaction A*, 1983, **14A**, 2375–2385.
8. Kuo, V. W. C. and Starke, E. A. Jr., The development of two texture variants and their effect on the mechanical behavior of a high strength P/M aluminum alloy, X7091. *Metallurgical Transaction A*, 1985, **16A**, 1089–1103.
9. Vasudévan, A. K. and Suresh, S., Lithium-containing aluminium alloys: cyclic fracture. *Metallurgical Transaction A*, 1985, **16A**, 475–477.
10. Bhargava, P. and Patterson, B. R., Quantitative characterization of indentation crack path in a cubic zirconia-10% vol alumina composite. *J. Am. Ceram. Soc.*, 1997, **80**, 1863–1867.
11. Holm, E. A., Surface formation energy for intergranular fracture in two-dimensional polycrystals. *J. Am. Ceram. Soc.*, 1998, **81**, 455–459.
12. Måløy, K. J., Hansen, A., Hinrichsen, E. L. and Roux, S., Experimental measurements of the roughness of brittle cracks. *Phys. Rev. Lett.*, 1992, **68**, 213–215.
13. Schmittbuhl, J., Roux, S. and Berthaud, Y., Development of roughness in crack propagation. *Europhys. Lett.*, 1994, **28**, 585–590.
14. Mecholsky, J J. Jr., Mackin, TJ. and Passoja, DE., Self-similar crack propagation in brittle materials. In *Advances in Ceramics, Vol. 22, Fractography of Glasses and Ceramics*, ed. J. R. Varner and V. D. Frechette, 1988, pp. 127–134.
15. Borodich, F. M., Some fractal models of fracture. *J. Mech. Phys. Solids*, 1997, **45**, 239–259.
16. Mosolov, A. B., Mechanics of fractal cracks in brittle solids. *Europhys. Lett.*, 1993, **24**, 673–678.
17. Theocaris, P. S. and Panagiotopoulos, P. D., Cracks of fractal geometry with unilateral contact and friction interface conditions. *Int. J. Fracture*, 1993, **60**, 293–310.
18. Heping, X., The fractal effect of irregularity of crack branching on the fracture toughness of brittle materials. *Int. J. Fracture*, 1989, **41**, 267–274.
19. Mandelbrot, B. B., Self-affine fractals and fractal dimension. *Physical Scripta*, 1985, **V32**, 257–260.
20. Mandelbrot, B. B., *Fractal: Form, Chance and Dimension*. W.H. Freeman, San Francisco, 1977.
21. Mandelbrot, B. B., *The Fractal Geometry of Nature*. W.H. Freeman, San Francisco, 1982.
22. Mandelbrot, B. B., Passoja, D. E. and Paulley, A. J., Fractal character of fracture surfaces of metals. *Nature*, 1984, **308**, 721–722.
23. Mecholsky, J. J. Jr., Passoja, D. E. and Feinberg-Ringel, K. S., Quantitative analysis of brittle fracture surfaces using fractal geometry. *J. Am. Ceram. Soc.*, 1989, **72**, 60–65.
24. Thompson, J. Y., Anusavice, K. J., Balasubramaniam, B. and Mecholsky, J. J. Jr., Effect of microcracking on the fracture toughness and fracture surface fractal dimension of lithia-based glass-ceramics. *J. Am. Ceram. Soc.*, 1995, **78**, 3045–3049.
25. Chen, C. T. and Runt, J., Fractal analysis of polystyrene fracture surfaces. *Polym. Commun.*, 1989, **30**, 334.
26. Mecholsky, J. J. Jr. and Freiman, S. W., Relationship between fractal geometry and fractography. *J. Am. Ceram. Soc.*, 1991, **74**, 3136–3138.
27. Bouchaud, E., Lapasset, G. and Planès, J., Fractal dimension of fractured surfaces: a universal value?. *Europhys. Lett.*, 1990, **13**, 73–79.
28. Baran, G. R., Roques-Carmes, C., Wehbi, D. and Degrange, M., Fractal characteristics of fracture surfaces. *J. Am. Ceram. Soc.*, 1992, **75**, 2687–2691.
29. Mecholsky, J. J. Jr. and Plaia, J. R., Fractal analysis on fracture surfaces of glass using replication techniques. *J. Non-Cryst. Solids*, 1992, **146**, 249–255.
30. Lange, F. F., Transformation toughening. Part 4 Fabrication, fracture toughness and strength of Al_2O_3-ZrO_2 composites. *J. Mater. Sci.*, 1982, **17**, 247–254.
31. Glass, S. J. and Green, D. J., Mechanical properties of infiltrated alumina-Y-TZP composites. *J. Am. Ceram. Soc.*, 1996, **79**, 2227–2236.
32. Green, D. J., Critical microstructures for microcracking in Al_2O_2-ZrO_2 composites. *J. Am. Ceram. Soc.*, 1982, **65**, 610–614.
33. Langlois, R. and Konsztowicz, K. J., Toughening in zirconia-toughened alumina composites with non-trasforming zirconia. *J. Mater. Sci. Lett.*, 1992, **11**, 1454–1456.

34. Hori, S., Yoshimura, M., Somiya, S., Kurita, R. and Kaji, H., Mechanical properties of ZrO_2-toughened Al_2O_3 ceramics from CVD powders. *J. Mat. Sci. Lett*., 1985, **4**, 413–416.
35. Li, J-F. and Watanabe, R., Fracture toughness of Al_2O_3-particle-dispersed Y_2O_3-partially stabilized zirconia. *J. Am. Ceram. Soc*., 1995, **78**, 1079–1082.
36. Srdic, V. and Radonjic, L., Processing of the alumina-zirconia composite and its mechanical properties. In *Third Euro-Ceramics*, Vol. 3, ed. P. Durán and J. F. Fernández, 1993, pp. 701–706.
37. Becher, P. F. and Swain, M. V., Grain-size-dependent transformation behavior in polycrystalline tetragonal zirconia. *J. Am. Ceram. Soc*., 1992, **75**, 493–502.
38. French, J. D., Chan, H. M., Harmer, M. P. and Miller, G. A., Mechanical properties of interpenetrating microstructures: the Al_2O_3/c-ZrO_2 system. *J. Am. Ceram. Soc*., 1992, **75**, 418–423.
39. Tomaszewski, H., Toughening effects in Al_2O_3-ZrO_2 system. *Ceram. Intern*., 1988, **14**, 117–125.
40. Underwood, E. E. and Banerji, K., Fractals in fractography. *Mater. Sci. Engin*., 1986, **80**, 1–14.
41. Underwood, E.E. and Banerji, K., Fractal analysis of fracture surfaces. In *ASM Handbook*, *Vol 12, Fractography*. ASM International, 1992, pp. 212–215.
42. Celli, A., Tucci, A. and Esposito, L., Quantitative evaluation by fractal analysis of indentation crack paths in Si_3N_4-SiC_w composites. *J. Eur. Ceram. Soc*., 1999, **19**, 441–449.
43. Celli, A., Tucci, A. and Esposito, L., Fractal analysis of cracks in Si_3N_4-SiC_w composites. *Silicates Industriels*, 1998, **63**, 93–99.
44. Salomoni, A., Tucci, A., Esposito, L. and Stamenkovic, I., Forming and sintering of multiphase bioceramics. *J. Mater. Sci. Materials in Medicine*, 1994, **5**, 651–653.
45. Chinn, R., Grain sizes of ceramics by automatic image analysis. *J. Am. Ceram. Soc*., 1994, **77**, 589–592.
46. Anstis, G. R., Chantikul, P., Lawn, B. R. and Marshall, D. B., A critical evaluation of indentation techniques for measuring fracture toughness: I, direct crack measurements. *J. Am. Ceram. Soc*., 1981, **64**, 533–538.
47. Mussler, B., Swain, M. V. and Claussen, N., Dependence of fracture toughness of alumina on grain size and test technique. *J. Am. Ceram. Soc*., 1982, **65**, 566–572.
48. Mecholsky, J. J. and Mackin, T. J., Fractal analysis of fracture in Ocala chert. *J. Mat. Sci. Lett*., 1988, **7**, 1145–1147.
49. Issa, M. A., Hammad, A. M. and Chudnovsky, A., Correlation between crack tortuosity and fracture toughness in cementitious material. *Int. J. Fracture*, 1993, **60**, 97–105.
50. Hill, J. H., Mecholsky, J. J. Jr. and Anusavice, K. J., Fractal analysis of toughening behavior in 3BaO5SiO_2 glass-ceramics. *J. Am. Ceram. Soc*., 2000, **83**, 545–552.
51. Passoja, D. E., Fundamental relationships between energy and geometry in fracture. In *Advanced in Ceramics, vol.22, Fractography of Glasses and Ceramics*, ed. J. R. Varner and V. D. Frechette, 1988, pp. 101–126.
52. Celli, A., Gutema, T., Bracali, P., Groppetti, R., Esposito, L. and Tucci, A., AFM, a tool for investigating indentation damage in ZrO_2. *Am. Ceram. Soc. Bull*., 1999, **78**, 87–91.
53. Kaliszewski, M. S., Behrens, G., Heuer, A. H., Shaw, M. C., Marshall, D. B., Dransmann, G. W., Steinbrech, R. W., Pajares, A., Guiberteau, F., Cumbrera, F. L. and Dominguez-Rodriguez, A., Indentation studies on Y_2O_3-stabilized ZrO_2: I, development of indentation-induced cracks. *J. Am. Ceram. Soc*., 1994, **77**, 1185–1193.